Field-Induced Dysprosium Single-Molecule Magnet Involving a Fused o-Semiquinone-Extended-Tetrathiafulvalene-o-Semiquinone Bridging Triad

Jessica Flores Gonzalez, Olivier Cador, Lahcène Ouahab, Sergey Norkov, Viacheslav Kuropatov, Fabrice Pointillart

inorganics

MDPI

Article

Field-Induced Dysprosium Single-Molecule Magnet Involving a Fused *o*-Semiquinone-Extended-Tetrathiafulvalene-*o*-Semiquinone Bridging Triad

Jessica Flores Gonzalez [1], Olivier Cador [1], Lahcène Ouahab [1], Sergey Norkov [2], Viacheslav Kuropatov [2,*] and Fabrice Pointillart [1,*]

1 Univ Rennes, CNRS, ISCR (Institut des Sciences Chimiques de Rennes)-UMR 6226, 35000 Rennes, France; jessica.flores-gonzales@univ-rennes1.fr (J.F.G.); olivier.cador@univ-rennes1.fr (O.C.); lahcene.ouahab@univ-rennes1.fr (L.O.)

2 G. A. Razuvaev Institute of Organometallic Chemistry of Russian Academy of Sciences, GSP-445, Tropinina str., 49, 603950 Nizhny Novgorod, Russia; x-outing-93@mail.ru

* Correspondence: viach@iomc.ras.ru (V.K.); fabrice.pointillart@univ-rennes1.fr (F.P.); Tel.: +33-(0)2-23-23-57-62 (F.P.); Fax: +33-(0)2-23-23-68-40 (F.P.)

Received: 27 March 2018; Accepted: 20 April 2018; Published: 3 May 2018

Abstract: The reaction between the 2,2′-benzene-1,4-diylbis(6-hydroxy-4,7-di-*tert*-butyl-1,3-benzodithiol-2-ylium-5-olate biradical triad (**L**) and the metallo-precursor $[Dy(hfac)_3]\cdot 2H_2O$ leads to the formation of a one-dimensional coordination polymer with the formula $\{[Dy(hfac)_3(\mathbf{L})]\cdot 2C_6H_{14}\}_n$ (**1**). The X-ray structure reveals that the polymeric structure is formed by the bridging of the $Dy(hfac)_3$ units with the multi-redox triad **L**. Single-crystal X-ray diffraction and UltraViolet-visible absorption spectroscopy confirm that the triad **L** in **1** is bound as a direduced, diprotonated form of *o*-quinone-extended tetrathiafulvalene-*o*-quinone (Q-exTTF-Q). Alternate Current (AC) measurements highlight a field-induced single-molecule magnet (SMM) behavior with an energy barrier of 20 K, and thus **1** can be described as a one-dimensional assembly of mononuclear SMMs bridged by the **L** triad.

Keywords: *o*-semiquinone; extended-tetrathiafulvalene; triads; lanthanides; single-molecule magnet

1. Introduction

Multifunctional materials are key systems for the communities of chemists and physicists studying exciting physical properties. One explored route to design multifunctional materials is the use of adequate organic ligands to contribute one property while metallic precursors carry additional properties such as magnetism and luminescence. To combine the two latter properties, lanthanide ions are the best candidates because of their intrinsic strong magnetic anisotropy and high magnetic moment combined with their specific luminescence [1–4]. Thus, a luminescent single-molecule magnet (SMM) [5–7], ferroelectric SMM [8], chiral SMM [9,10], and redox-active SMM [11,12] were obtained, associating chiral or redox-active ligands with lanthanide precursors. Following this strategy, one of the most widely used redox-active ligands is based on the tetrathiafulvalene (TTF) core. Even more interesting is the decoration of the TTF core with one or two *p*-quinone [13,14] and *o*-quinone molecules [15], because these can be easily oxidized or reduced in the coordination sphere of the metal, leading to the observation of a redox-isomerisation mechanism [16,17]. The resulting donor (D)-acceptor (A) dyads or A-D-A triads (where D refers to TTF and A refers to quinone) open the route for potential applications in molecular electronics and optoelectronics because of their low highest occupied molecular orbital to lowest unoccupied molecular orbital (HOMO–LUMO) gap [18]. A few

years ago, some of the current authors elaborated upon dinuclear complexes that displayed SMMs or luminescence using the 4,4′,7,7′-tetra-*tert*-butyl-2,2′-bi-1,3-benzodithiole-5,5′,6,6′-tetrone triad [19,20].

Along these lines, we proposed to replace the TTF core with *p*-phenylene-extended TTF to lower the HOMO–LUMO gap, because the first oxidation potential is lower than for TTF [21], and to stabilize the protonated semiquinone form, which might offer a dissymmetric coordination site and thus give the possibility to reach new molecular systems. The coordination reaction between $[Dy(hfac)_3]\cdot 2H_2O$ ($hfac^-$ refers to 1,1,1,5,5,5-hexafluoroacetylacetonate) and the 2,2′-benzene-1,4-diylbis(6-hydroxy-4,7-di-*tert*-butyl-1,3-benzodithiol-2-ylium-5-olate biradical triad [22] (**L**) (Scheme 1) led to the formation of the $\{[Dy(hfac)_3(\mathbf{L})]\cdot 2C_6H_{14}\}_n$ (**1**) polymer. The X-ray structure and photo-physical and magnetic properties were studied.

2. Results and Discussion

2.1. Synthesis

The 2,2′-benzene-1,4-diylbis(6-hydroxy-4,7-di-*tert*-butyl-1,3-benzodithiol-2-ylium-5-olate biradical triad (**L**) (Scheme 1) was previously synthesized starting from a 2:1 4-chloro-3,6-di-*tert*-butyl-*o*-benzoquinone and sodium tetrathioterephthalate mixture in tetrahydrofuran (THF) [22]. This triad was previously studied by open-shell density functional theory calculations, which revealed that the broken-symmetry (BS) state in a global minimum is singlet biradical according to the spin density distribution. The value of the antiferromagnetic coupling between the two semiquinone radical centers was estimated as 1092 cm^{-1} [23]. Consequently the biradical triad **L** is Electronic Paramagnetic Resonance (EPR) silent [23].

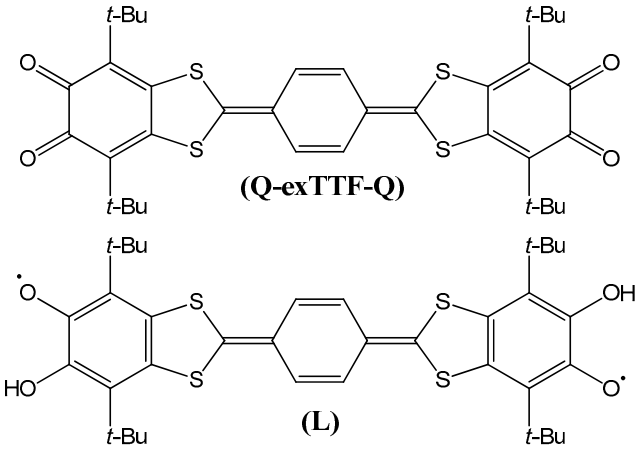

Scheme 1. Molecular structure of the triads Q-exTTF-Q and biradical **L**.

The coordination reaction between an equimolar ratio of the $[Dy(hfac)_3]\cdot 2H_2O$ metallo-precursor and the **L** triad leads to the formation of dark blue–purple single crystals of $\{[Dy(hfac)_3(\mathbf{L})]\cdot 2C_6H_{14}\}_n$ (**1**) after the slow diffusion of *n*-hexane in the dark.

2.2. Crystal Structure Description of $\{[Dy(hfac)_3(L)]\cdot 2C_6H_{14}\}_n$ (1)

Compound **1** crystallizes in the $P2_1/c$ (N°14) monoclinic space group (Table 1). The asymmetric unit is composed of one $Dy(hfac)_3$ moiety, one **L** triad and two *n*-hexane molecules of crystallization. An Oak Ridge thermal ellipsoid plot (ORTEP) view of **1** is depicted in Figure S1.

The X-ray structure of **1** reveals the formation of a coordination polymer (Figure 1). The coordination between the Dy^{III} ion and the bridging ligand takes place through the non-protonated oxygen atoms (O1 and O4). The two protonated oxygen atoms (O2 and O3) remain uncoordinated. The bridging ligand in **1** is almost planar, and its structure is very similar to that of the free ligand in its protonated

semiquinone form [22]. In fact, the torsion angle between the planes defined by the benzo-1,3-dithio system and the *p*-phenylene ring takes the average value of 6.32(11)°, which can be compared with the value of 8.70(10)° found for the free **L** ligand. The direduced, diprotonated form of the ligand **L** in **1** was also confirmed by the distribution of C–C distances in the dioxolene rings as well as the C–OH (1.347(4) Å) and C–O· (1.307(4) Å) bond lengths. The C–OH and C–O· distances in **1** were slightly longer and shorter, respectively, than in the free biradical triad because of the electronic effect of the coordination of the trivalent metal. Finally, the semiquinone form was also confirmed by absorption spectroscopy (see Section 2.3). The arrangement of the ligands around the Dy^{III} center leads to an O_8 surrounding with a coordination polyhedron symmetry intermediate between the C_{2v} biaugmented trigonal prism ($CShM_{BTPR-8}$ = 1.140), the D_{4d} square antiprism ($CShM_{SAPR-8}$ = 1.191), and the D_{2d} triangular dodecahedron ($CShM_{TDD-8}$ = 1.238). The numbers correspond to the deviation from the ideal symmetries determined with the *SHAPE* 2.1 program [24]. The Dy1–O_{hfac} distances (2.382(3) Å) were longer than those of Dy1–O_{SQ} (2.267(3) Å) (Table 2).

Table 1. X-ray crystallographic data for **1**.

Compound	**{[Dy(hfac)$_3$(L)]·2C$_6$H$_{14}$}$_n$ (1)**
Formula	$C_{63}H_{73}DyF_{18}O_{10}S_4$
M/g·mol^{-1}	1622.95
Crystal system	Monoclinic
Space group	$P2_1/c$ (N°14)
Cell parameters	a = 15.8351(14) Å b = 23.8650(20) Å c = 19.0098(19) Å
Volume/Å^3	7047.4(11)
Z	4
T/K	150(2)
2θ range/°	$5.97 \leq 2\theta \leq 50.48$
ϱ_{calc}/g cm^{-3}	1.530
μ/mm^{-1}	1.280
Number of reflections	62,952
Independent reflections	16,127
R_{int}	0.0608
$Fo^2 > 2\sigma(Fo)^2$	12,302
Number of variables	813
R_1, wR_2	0.0436, 0.1003

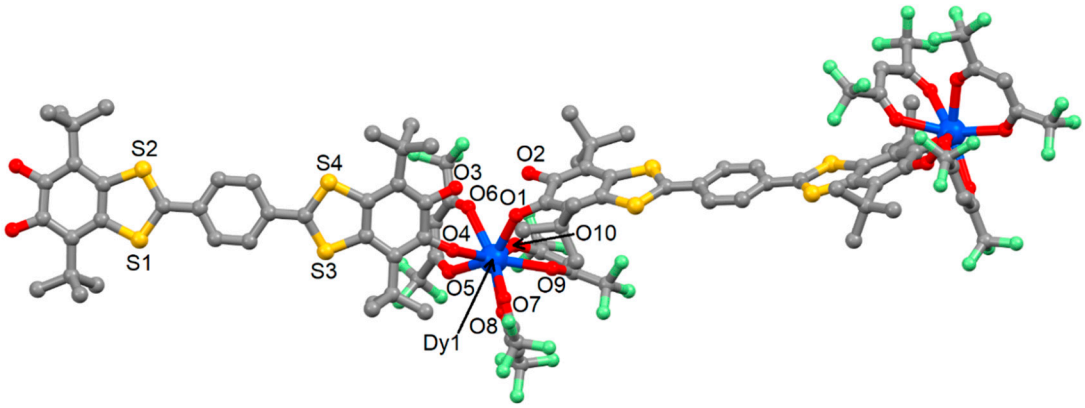

Figure 1. ORTEP view of **1**. Thermal ellipsoids are drawn at 30% probability. Hydrogen atoms and solvent molecules of crystallization are omitted for clarity.

The crystal packing of **1** is shown in Figure 2. No significant intermolecular interactions, such as S···S, S···O, or π···π interactions, as observed in the X-ray structure of the free ligand **L** [22], were

identified. The **L** triad and Dy(hfac)$_3$ metallo-precursor formed two subnetworks aligned along the *c*-axis (Figure 2). The shortest intra- and inter-molecular Dy···Dy distances were determined to be equal to 21.079 and 11.079 Å, respectively.

Table 2. Selected bond lengths (Å) for compound **1**.

Compound	1
Dy1–O1	2.296(3)
Dy1–O4	2.237(3)
Dy1–O5	2.360(3)
Dy1–O6	2.430(3)
Dy1–O7	2.370(3)
Dy1–O8	2.389(3)
Dy1–O9	2.395(3)
Dy1–O10	2.346(3)

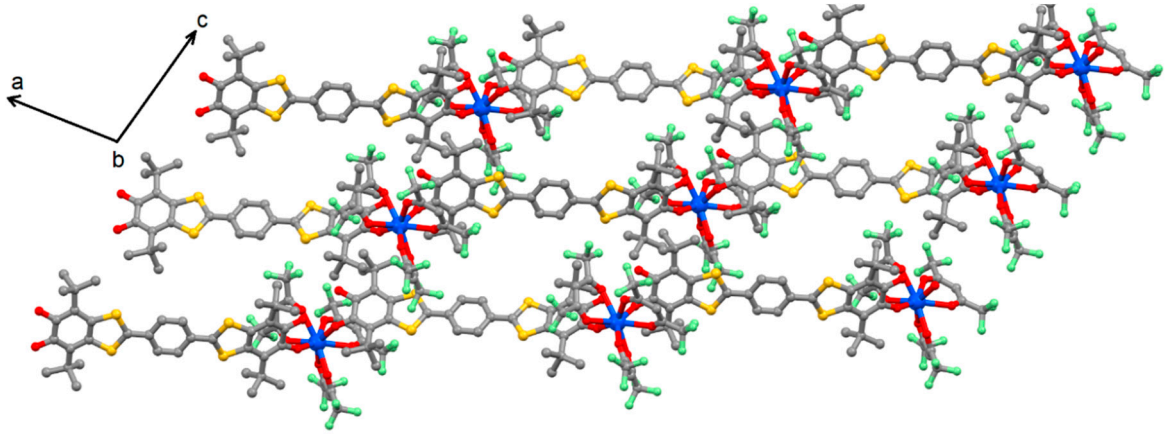

Figure 2. Crystal packing of **1** in the plan [101].

2.3. Infrared Spectroscopy

The Infrared (IR) spectra for both the free **L** ligand and **1** were recorded in the KBr solid state. The protonated semiquinone form of **L** was confirmed by C–O· vibrations at 1549 and 1502 cm^{-1} [22]. For **1**, these semiquinone carbonyl vibrations were identified in the frequency range of 1485–1565 cm^{-1}. The red shift is explained by the coordination of the Dy(hfac)$_3$ moiety, and this was in good agreement with the slight changes in bond lengths observed in the X-ray structure. The additional strong band centered at 1655 cm^{-1} was attributed to the C=O carbonyl groups of the hfac$^-$ anions. As previously observed [22], the characteristic signals of hydroxyl groups were observed for neither **L** nor **1**.

2.4. Absorption Spectroscopy

The absorption spectrum of **1** was recorded in CH_2Cl_2 solution at room temperature (Figure 3). It displayed a broad absorption band in the near infrared (NIR) region (890 nm), which should correspond to HOMO to LUMO excitations [22]. Such a wavelength is characteristic of the semiquinone form of the triad in **1**, whereas in the case of the quinone form, it should be centered at 750 nm [22]. The less-intense absorption band centered at 540 nm was attributed to the α+β-SOMOs to LUMO+1 excitations for the free **L** [22]. Clear changes in the electronic spectrum of **1** were observed compared to that of the free triad. Thus, more excitations were observed in both the NIR and visible regions likely as a result of the desymmetrization of the triad after complexation. Nevertheless, the most important difference between the electronic spectra of free **L** and **1** was the intensity of the absorption band centered near 300 nm. This absorption band originated from the π–π* excitations localized on the hfac$^-$ anions [25].

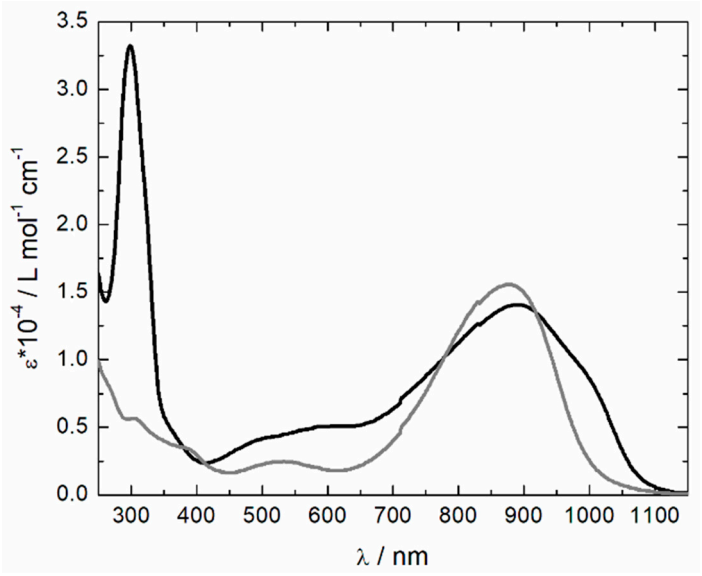

Figure 3. Electronic spectra of **L** (gray line) and **1** (black line) in CH_2Cl_2 ($c = 5 \times 10^{-5}$ M).

2.5. Magnetic Properties

The temperature dependence of the $\chi_M T$ product for **1** is depicted in Figure 4a. The room temperature $\chi_M T$ value was 13.95 $cm^3 \cdot K \cdot mol^{-1}$, which was in good agreement with the expected value of 14.17 $cm^3 \cdot K \cdot mol^{-1}$ for a magnetically isolated Dy^{III} ion ($^6H_{15/2}$ with g = 4/3) [26]. It is worth noting that the magnetic contribution from the two semiquinone radicals was not observed because, even at room temperature, they were strongly antiferromagnetically coupled (1092 cm^{-1}). Upon cooling, the $\chi_M T(T)$ curve monotonically decreased until 2 K. At this temperature, the $\chi_M T$ product reached the value of 11.84 $cm^3 \cdot K \cdot mol^{-1}$. The reason for such behavior is the thermal depopulation of the ligand field levels (M_J combination) in the ground state multiplet. In the inset of Figure 4a is depicted the field dependence of the magnetization. At 50 kOe, the magnetization reached a value of 5.30 Nβ, in agreement with the expected value of 5 Nβ for an Ising ground state.

An out-of-phase signal of the magnetic susceptibility (χ_M") was observed at a high frequency (1000 Hz) at 2 K in a zero-Direct Current (DC) magnetic field (Figure 4b and Figure S2). Nevertheless, no maxima were visible in the experimental time window available with our magnetometer because of an efficient zero-field quantum tunneling of the magnetization (QTM), which allows a fast relaxation as usually observed for mononuclear SMMs of Dy^{III} [27,28]. In order to suppress the QTM, a DC magnetic field was applied, and a scan field of the magnetic susceptibility at 2 K was performed (Figure 4b). The application of a small DC field shifts the maxima of the χ_M" to lower frequencies. Such a shift is a sign of the suppression of the zero-field QTM [29,30], dipolar interaction [31], and/or hyperfine interaction [32,33], as well as of the breaking of the transverse magnetic anisotropy [34].

Sample **1** highlighted the frequency dependence of the out-of-phase component of the magnetic susceptibility under the optimal DC magnetic field of 1200 Oe (Figures 4c and S3). The relaxation times were extracted using an extended Debye model ($\tau^{-1} = {\tau_0}^{-1} \exp(-\Delta/T)$) from the Cole–Cole plot [35] (Figure S4), giving the resulting Arrhenius plot shown in Figure 4d. The Arrhenius plot was fitted using only an Orbach relaxation, which provided an energy barrier of Δ = 13.3(3) cm^{-1} and $\tau_0 = 2.14(20) \times 10^{-5}$ s. The Arrhenius plot deviated from the linearity at a low temperature, suggesting the coexistence of more than one relaxation process; thus the existence of Raman [36–40] and/or Direct [36–40] processes cannot be excluded.

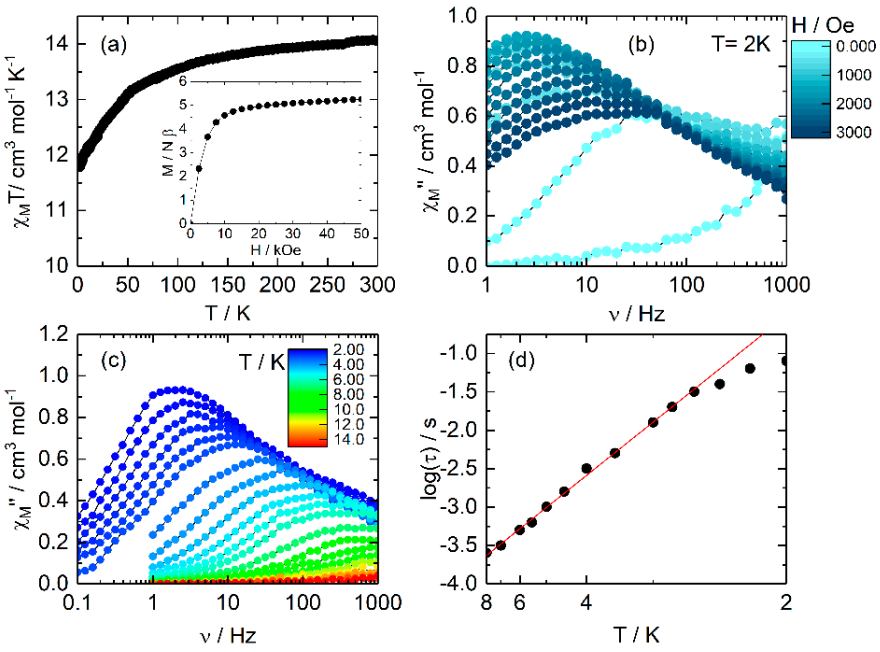

Figure 4. (**a**) Thermal dependence of $\chi_M T$ for **1**. Inset: field variation of the magnetization measured at 2 K; (**b**) Scan field of the frequency dependence of the magnetic susceptibility; (**c**) Frequency dependence of the out-of-phase signal of the magnetic susceptibility measured under a DC applied magnetic field of 1200 Oe; (**d**) Arrhenius plot of the temperature variation of the relaxation time measured in a DC applied magnetic field of 1200 Oe (full circles) with the best fitted curve (red line) in the temperature range of 2–8 K.

3. Experimental Section

3.1. Synthesis

General Procedures and Materials. The precursors Dy(hfac)$_3$·2H$_2$O (hfac$^-$ = 1,1,1,5,5,5-hexafluoroacetylacetonate anion) [41] and the 2,2′-benzene-1,4-diylbis(6-hydroxy-4,7-di-*tert*-butyl-1,3-benzodithiol-2-ylium-5-olate biradical triad [22] (**L**) were synthesized following previously reported methods. All other reagents were purchased from Aldrich Co., Ltd. (Saint-Quentin Fallavier, France) and were used without further purification.

*3.2. Synthesis of Complex {[Dy(hfac)$_3$(L)]·2C$_6$H$_{14}$}$_n$ (**1**)*

Dy(hfac)$_3$·2H$_2$O (0.04 mmol, 32.8 mg) was dissolved in 10 mL of CH_2Cl_2 and then added to a solution of 10 mL of CH_2Cl_2 containing 26.4 mg of **L** (0.04 mmol). After 15 min of stirring, 20 mL of *n*-hexane was layered at room temperature in the dark. Slow diffusion leads to dark purple–blue single crystals, which are suitable for X-ray studies. Yield (determined from isolated single crystals): 28.6 mg (44%). Anal. Calcd (%) for $C_{63}H_{73}DyF_{18}O_{10}S_4$: C 46.58, H 4.50; found: C 45.99, H 4.42. I.R. (KBr): 2965 (w), 2885 (w), 1655 (s), 1565 (w), 1554 (m), 1533 (m), 1511 (m), 1499 (m), 1481 (m), 1409 (s), 1387 (s), 1363 (m), 1257 (s), 1203 (w), 1144 (s), 1099 (w), 861 (w), 798 (w), 660 (m), and 585 (w) cm^{-1}.

3.3. Crystallography

Single crystals of **1** were mounted on a APEXIII D8 VENTURE Bruker-AXS diffractometer (Bruker, Billerica, MA, USA) for data collection (Mo Kα radiation source, λ = 0.71073 Å), from the Centre de Diffractométrie (CDIFX), Université de Rennes 1, France. Structures were solved with a direct method using the *SHELXT* program [42] and were refined with a full matrix least-squares method on F^2 using the *SHELXL*-14/7 program [43]. Crystallographic data are summarized in Table 1. Complete crystal

structure results as a CIF file including bond lengths, angles, and atomic coordinates are given in the Supplementary Materials (CCDC number 1825935).

3.4. Physical Measurements

The elementary analyses of the compounds were performed at the Centre Régional de Mesures Physiques de l'Ouest, Rennes. Absorption spectra were recorded on a Varian Cary 5000 UV-Visible–NIR spectrometer (Varian Inc. (Agilent Technologies), Palo Alto, CA, USA) equipped with an integration sphere. The DC magnetic susceptibility measurements were performed on solid polycrystalline samples with a Quantum Design MPMS-XL SQUID magnetometer (Quantum Design Inc., CA, USA) for temperatures between 2 and 300 K under an applied magnetic field of 200 Oe, between 2 and 20 K for 2 kOe, and between 20 and 80 K for 10 kOe and above. These measurements were all corrected for the diamagnetic contribution as calculated with Pascal's constants.

4. Conclusions and Outlook

A one-dimensional coordination polymer with the formula $\{[Dy(hfac)_3(\mathbf{L})]\cdot 2C_6H_{14}\}_n$ (**1**) was synthesized. Its X-ray structure revealed that the $Dy(hfac)_3$ unit is bridged by the **L** biradical triad through the monodentate coordination of C–O· only. The bond-length distribution analysis, IR, and UV-vis absorption spectroscopy data confirm that the Q-exTTF-Q triad in **1** exists in a direduced, diprotonated state. The last technique highlighted the two expected HOMO–LUMO intra-ligand charge-transfer and α+β-SOMOs to LUMO+1 excitations for the semiquinone form. The AC measurements indicated field-induced SMM behavior with an energy barrier of 13.3 cm^{-1}. The coordination polymer **1** can be described as a one-dimensional assembly of mononuclear SMMs bridged by the **L** triad. The triad **L** is a multi-redox active ligand for which the two semiquinone moieties can be either reduced into a catechol or oxidized into an *o*-quinone form; consequently such redox activity is expected to strongly influence the magnetic properties of the polymer. Such a study is under progress in our laboratory.

Supplementary Materials: The following are available online at http://www.mdpi.com/2304-6740/6/2/45/s1: CIF and CIF-checked file; Figure S1: ORTEP View of the asymmetric unit of **1**; Figure S2: Frequency dependence of the in-phase and out-of-phase signal of the magnetic susceptibility measured under a zero DC applied magnetic field; Figure S3: Frequency dependence of the in-phase signal of the magnetic susceptibility measured under a DC applied magnetic field of 1200 Oe; Figure S4: Normalized Cole–Cole plots for **1** at several temperatures between 2 and 8 K.

Author Contributions: S.N., V.K. and F.P. made the synthesis, J.F.G. and O.C. performed the magnetic and electronic spectra measurements and interpreted them. All authors participated to the writing process of the manuscript. All authors read and approved the final version of the manuscript.

Acknowledgments: This work was supported by the CNRS, Rennes Métropole, Université de Rennes 1, Région Bretagne, FEDER, Agence Nationale de la Recherche (N° ANR-13-BS07-0022-01), European Research Council (ERC, N°725184) and the Russian state assignment (Theme 44.1, Reg. No. 0094-2017-0009).

Conflicts of Interest: The authors declare no conflict of interest.

References

1. Benelli, C.; Gatteschi, D. Magnetism of Lanthanides in Molecular Materials with Transition-Metal Ions and Organic Radicals. *Chem. Rev.* **2002**, *102*, 2369–2388. [CrossRef] [PubMed]
2. Sessoli, R.; Powell, A.K. Strategies towards single molecule magnets based on lanthanide ions. *Coord. Chem. Rev.* **2009**, *253*, 2328–2341. [CrossRef]
3. Woodruff, D.N.; Winpenny, R.E.P.; Layfield, R.A. Lanthanide single-molecule magnets. *Chem. Rev.* **2013**, *113*, 5110–5148. [CrossRef] [PubMed]
4. Bünzli, J.-C.G.; Piguet, C. Taking advantage of luminescent lanthanide ions. *Chem. Soc. Rev.* **2005**, *34*, 1048–1077. [CrossRef] [PubMed]

5. Li, X.-L.; Chen, C.-L.; Xiao, H.-P.; Wang, A.-L.; Liu, C.-M.; Zheng, X.; Gao, L.-J.; Yanga, X.-G.; Fang, S.-M. Luminescent, magnetic and ferroelectric properties of noncentrosymmetric chain-like complexes composed of nine-coordinated lanthanide ions. *Dalton Trans.* **2013**, *42*, 15317–15325. [CrossRef] [PubMed]
6. Soussi, K.; Jung, J.; Pointillart, F.; Le Guennic, B.; Lefeuvre, B.; Golhen, S.; Cador, O.; Guyot, Y.; Maury, O.; Ouahab, L. Magnetic and photo-physical inverstigations into Dy^{III} and Yb^{III} complexes involving tetrathiafulvalene ligand. *Inorg. Chem. Front.* **2015**, *2*, 1105–1117. [CrossRef]
7. Cucinotta, G.; Perfetti, M.; Luzon, J.; Etienne, M.; Car, P.E.; Caneschi, A.; Calvez, G.; Bernot, K.; Sessoli, R. Magnetic Anisotropy in a Dysprosium/DOTA Single-Molecule Magnet: Beyond Simple Magneto-Structural Correlations. *Angew. Chem. Int. Ed.* **2012**, *51*, 1606–1610. [CrossRef] [PubMed]
8. Long, J.; Rouquette, J.; Thibaud, J.-M.; Ferreira, R.A.S.; Carlos, L.D.; Donnadieu, B.; Vieru, V.; Chibotaru, L.F.; Konczewicz, L.; Haines, J.; et al. A high-Temperature Molecular Ferroelectric Zn/Dy Complex Exhibiting Single-Ion-Magnet Behavior and Lanthanide Luminescence. *Angew. Chem. Int. Ed.* **2015**, *54*, 2236–2240. [CrossRef] [PubMed]
9. Lin, S.-Y.; Wang, C.; Zhao, L.; Wua, J.; Tang, J. Chiral mononuclear lanthanide complexes and the field-induced single-ion magnet behavior of a Dy analogue. *Dalton Trans.* **2015**, *44*, 223–229. [CrossRef] [PubMed]
10. Ou-Yang, J.-K.; Saleh, N.; Fernandez Garcia, G.; Norel, L.; Pointillart, F.; Guizouarn, T.; Cador, O.; Totti, F.; Ouahab, L.; Crassous, J.; et al. Improved slow magnetic relaxation in optically pure helicene-based Dy^{III} single molecule magnets. *Chem. Commun.* **2016**, *52*, 14474–14477. [CrossRef] [PubMed]
11. Pointillart, F.; Le Guennic, B.; Golhen, S.; Cador, O.; Ouahab, L. Slow magnetic relaxation in radical cation tetrathiafulvalene-based lanthanide(III) dinuclear complexes. *Chem. Commun.* **2013**, *49*, 11632–11634. [CrossRef] [PubMed]
12. Pointillart, F.; Golhen, S.; Cador, O.; Ouahab, L. Slow Magnetic Relaxation in a Redox-Active Tetrathiafulvalene-Based Ferromagnetic Dusprosium Complex. *Eur. J. Inorg. Chem.* **2014**, *2014*, 4558–4563. [CrossRef]
13. Rovira, C.; Hudhomme, P. Intramolecular electron transfer mediated by a tetrathiafulvalene bridge in a purely organic mixed-valence system. *Angew. Chem. Int. Ed.* **2003**, *42*, 2765–2768.
14. Dumur, F.; Gautier, N.; Gallego-Planas, N.; Sahin, Y.; Levillain, E.; Mercier, N.; Hudhomme, P. Novel Fused D-A Dyad and A-D-A Triad Incorporating Tetrathiafulvalene and *p*-Benzoquinone. *J. Org. Chem.* **2004**, *69*, 2164–2177. [CrossRef] [PubMed]
15. Kuropatov, V.; Klementieva, S.; Fukin, G.; Mitin, A.; Ketlov, S.; Budnikova, Y.; Cherkasov, V.; Abakumov, G. Novel method for the synthesis of functionalized tetrathiafulvalenes, an acceptor–donor–acceptor molecule comprising of two *o*-quinone moieties linked by a TTF bridge. *Tetrahedron* **2010**, *66*, 7605–7611. [CrossRef]
16. Abakumov, G.A.; Nevodchikov, V.I. Thermomechanical and Photomechanical Effects in the Crystals of Complexes with Free Radicals. *Dokl. Akad. Nauk SSSR* **1982**, *266*, 1407–1410.
17. Abakumov, G.A.; Nevodchikov, V.I.; Cherkasov, V.K. A reversible intramolecular metal-ligand electron transfer in *o*-semiquinonate rhodium complexes. A redox-isomerism in paramagnetic metal complexes. *Dokl. Akad. Nauk SSSR* **1984**, *278*, 641–645.
18. Perepichka, D.F.; Bryce, M. Molecules with exceptionally small HOMO–LUMO gaps. *Angew. Chem. Int. Ed.* **2005**, *44*, 5370–5373. [CrossRef] [PubMed]
19. Pointillart, F.; Klementieva, S.; Kuropatov, V.; Le Gal, Y.; Golhen, S.; Cador, O.; Cherkasov, V.; Ouahab, L. A single molecule magnet behavior in a D3h symmetry Dy(III) complex involving a quinone-tetrathiafulvalene-quinone bridge. *Chem. Commun.* **2012**, *48*, 714–716. [CrossRef] [PubMed]
20. Pointillart, F.; Kuropatov, V.; Mitin, A.; Maury, O.; Le Gal, Y.; Golhen, S.; Cador, O.; Cherkasov, V.; Ouahab, L. Lanthanide-Based Dinuclear Complexes Involving an *o*-Quinone-Tetrathiafulvalene-*o*-Quinone Bridging Ligand: X-ray Structures, Magnetic and Photophysical Properties. *Eur. J. Inorg. Chem.* **2012**, *2012*, 4708–4718. [CrossRef]
21. Yamashita, Y.; Kobayashi, Y.; Miyashi, T. p-Quinodimethane Analogues of Tetrathiafulvalene. *Angew. Chem. Int. Ed.* **1989**, *28*, 1052–1053. [CrossRef]
22. Chalkov, N.O.; Cherkasov, V.K.; Abakumov, G.A.; Romanenko, G.V.; Ketkov, S.Y.; Smolyaninov, I.V.; Starikov, A.G.; Kuropatov, V.A. Compactly Fused *o*-Quinone-Extended Tetrathiafulvalene-*o*-Quinone Triad—A Redox-Amphoteric Ligand. *Eur. J. Org. Chem.* **2014**, *2014*, 4571–4576. [CrossRef]

23. Chalkov, N.O.; Cherkasov, V.K.; Abakumov, G.A.; Starikov, A.G.; Kuropatov, V.A. Protonated paramagnetic redox forms of di-*o*-quinone bridged with *p*-phenylene-extended TTF: A EPR spectroscopy study. *Beilstein J. Org. Chem.* **2016**, *12*, 2450–2456. [CrossRef] [PubMed]
24. Llunell, M.; Casanova, D.; Cirera, J.; Bofill, J.M.; Alemany, P.; Alvarez, S. *SHAPE (v. 2.1)*; University of Barcelona: Barcelona, Spain, 2013.
25. Pointillart, F.; Cauchy, T.; Maury, O.; Le Gal, Y.; Golhen, S.; Cador, O.; Ouahab, L. Tetrathiafulvalene-amido-2-pyridine-N-oxide as Efficient Charge-Transfer Antenna Ligand for the sensitization of Yb^{III} Luminescence in a Series of Lanthanide Paramagnetic Coordination Complexes. *Chem. Eur. J.* **2010**, *16*, 11926–11941. [CrossRef] [PubMed]
26. Kahn, O. *Molecular Magnetism*; VCH: Weinhem, Germany, 1993.
27. Da Cunha, T.T.; Jung, J.; Boulon, M.-E.; Campo, G.; Pointillart, F.; Pereira, L.M.; Le Guennic, B.; Cador, O.; Bernot, K.; Pineider, F.; et al. Magnetic Poles Determinations and Robustness of Memory Effect upon Solubilization in a Dy^{III}-Based Single Ion Magnet. *J. Am. Chem. Soc.* **2013**, *135*, 16332–16335. [CrossRef] [PubMed]
28. Latendresse, P.T.; Bhuvanesh, S.N.; Nippe, M. Slow Magnetic Relaxation in a Lanthanide-[1] Metallocenophane Complex. *J. Am. Chem. Soc.* **2017**, *139*, 8058–8061. [CrossRef] [PubMed]
29. Gatteschi, D.; Sessoli, R. Quantum Tunneling of Magnetization and Related Phenomena in Molecular Materials. *Angew. Chem. Int. Ed.* **2003**, *42*, 268–297. [CrossRef] [PubMed]
30. Ishikawa, N.; Sugita, M.; Wernsdorfer, W. Quantum Tunneling of Magnetization in Lanthanide Single-Molecule Magnets: Bis(phthalocyaninato)terbium and Bis(phthalocyaninato)dysprosium Anions. *Angew. Chem. Int. Ed.* **2005**, *44*, 2931–2935. [CrossRef] [PubMed]
31. Guo, Y.-N.; Xu, G.-F.; Wernsdorfer, W.; Ungur, L.; Guo, Y.; Tang, J.; Zhang, H.-J.; Chibotaru, L.F.; Powell, A.K. Strong axiality and ising exchange interaction suppress zero-field tunneling of magnetization of an asymmetric Dy2 single-molecule magnet. *J. Am. Chem. Soc.* **2011**, *133*, 11948–11951. [CrossRef] [PubMed]
32. Ishikawa, N.; Sugita, M.; Wernsdorfer, W. Nuclear Spin Driven Quantum Tunneling of Magnetization in a New Lanthanide Single-Molecule Magnet: Bis(Phthalocyaninato)holmium Anion. *J. Am. Chem. Soc.* **2005**, *127*, 3650–3651. [CrossRef] [PubMed]
33. Pointillart, F.; Bernot, K.; Golhen, S.; Le Guennic, B.; Guizouarn, T.; Ouahab, L.; Ouahab, L. Magnetic Memory in an Isotopically Enriched and Magnetically Isolated Mononuclear Dysprosium Complex. *Angew. Chem. Int. Ed.* **2015**, *54*, 1504–1507. [CrossRef] [PubMed]
34. Ungur, L.; Chibotaru, L.F. Magnetic anisotropy in the excited states of low symmetry lanthanide complexes. *Phys. Chem. Chem. Phys.* **2011**, *13*, 20086–20090. [CrossRef] [PubMed]
35. Cole, K.S.; Cole, R.H. Dispersion and absorption in dielectrics I. Alternating current characteristics. *J. Chem. Phys.* **1941**, *9*, 341–351. [CrossRef]
36. Orbach, R. Spin-lattice relaxation in rare-earth salts. *Proc. R. Soc. A* **1961**, *264*, 458–484. [CrossRef]
37. Orbach, R. On the theory of spin-lattice relaxation in paramagnetic salts. *Proc. Phys. Soc.* **1961**, *77*, 821–826. [CrossRef]
38. Abragam, A.; Bleaney, B. *Electron Paramagnetic Resonance of Transition Ions*; Clarendon Press: Oxford, UK, 1970.
39. Shrivastava, K.N. Theory of spin–lattice relaxation. *Phys. Status Solidi* **1983**, *117*, 437–458. [CrossRef]
40. Scott, P.L.; Jeffries, C.D. Spin-lattice relaxation in some rare-earth salts at helium temperatures; observation of the phonon bottleneck. *Phys. Rev.* **1962**, *127*, 32–51. [CrossRef]
41. Richardson, M.F.; Wagner, W.F.; Sands, D.E. Rare-earth trishexafluoroacetylacetonates and related compounds. *J. Inorg. Nucl. Chem.* **1968**, *30*, 1275–1289. [CrossRef]
42. Sheldrick, G.L. *SHELXT*—Integrated space-group and crystal-structure determination. *Acta Crystallogr. Sect. A* **2015**, *71*, 3–8. [CrossRef] [PubMed]
43. Sheldrick, G.M. Crystal structure refinement with *SHELXL*. *Acta Crystallogr. Sect. C* **2015**, *71*, 3–8.